AIAA JOURNAL
Vol. 31, No. 5, May 1993

Nonlinear Large Amplitude Vibration of Composite Helicopter Blade at Large Static Deflection

Taehyoun Kim* and John Dugundji†
Massachusetts Institute of Technology, Cambridge, Massachusetts 02139

The nonlinear, large amplitude nonrotating free vibration of composite helicopter blades under large static deflection is investigated analytically and experimentally. A new model capable of handling large amplitudes as well as large deflections was developed based on the use of Euler angles and a harmonic balance, finite difference solution of the basic large deflection equations. The behavior of the first and second bending, the first fore-and-aft, and the first torsional modes of $[0/90]_{3S}$ and $[45/0]_S$ graphite/epoxy flat beams were explored analytically as tip static deflection and tip amplitudes vary. Free vibration tests of several different lay-ups of composite blades show good agreement between theory and experiment. It is found that both large static deflection and large amplitudes can affect the fore-and-aft and torsional modes significantly, but bending modes are not influenced much by the geometrical nonlinearities.

Nomenclature

c	= chord
$[E]$	= beam stress-strain stiffness matrix
E	= Young's modulus
F_1, F_2, F_3	= force resultant components in local axes
F_x, F_y, F_z	= force resultant components in global axes
G	= shear modulus
I_p	= beam mass moment of inertia about ξ axis
I_η	= beam area moment of inertia about ζ axis
I_ζ	= beam area moment of inertia about η axis
J	= beam torsion constant
L	= beam length
M_x, M_y, M_z	= moment resultant components in global axes
M_1, M_2, M_3	= moment resultant components in local axes
m	= beam mass per unit length
m_x, m_y, m_z	= applied moment components in global axes
m_{xT}, m_{yT}, m_{zT}	= total applied moment components in global axes
m_1, m_2, m_3	= applied moment components in local axes
m_G	= applied moment vector in global axes
p_x, p_y, p_z	= applied load components in global axes
p_{xT}, p_{yT}, p_{zT}	= total applied load components in global axes
p_1, p_2, p_3	= applied load components in local axes
p_G	= applied load vector in global axes
p_L	= applied load vector in local axes
s	= arc length
$[T]$	= transformation matrix
u, v, w	= displacements along x, y, z axes
w_t	= static tip deflection
x, y, z	= global coordinates
$\gamma_{\xi\eta}, \gamma_{\xi\zeta}$	= beam shear strains
ϵ	= beam extension strain or a small parameter
$[\kappa]$	= curvature matrix
κ_ξ	= twist rate around ξ axis
$\kappa_\eta, \kappa_\zeta$	= bending curvatures around η, ζ axes
ξ, η, ζ	= local coordinates
ϕ	= total twist angle $= \int_0^s \kappa_\xi \, ds$
ψ, β, θ	= Euler angles
ω	= frequency

Subscripts

o	= mean
s	= sine components

Presented as Paper 91-1221 at the AIAA/ASME/ASCE/AHS/ASC Structures, Structural Dynamics, and Materials Conference, Baltimore, MD, April 8-10, 1991; received May 14, 1991; revision received Aug. 11, 1992; accepted for publication Aug. 17, 1992.

*Research Assistant, Department of Aeronautics and Astronautics; currently Post-Doctoral Fellow, Computational Mechanics Center, Atlanta, GA 30332. Member AIAA.

†Professor, Department of Aeronautics and Astronautics. Member AIAA.

Introduction

IT is known that under large static deflections, natural frequencies and mode shapes of helicopter blades, particularly those of the fore-and-aft (lead-lag) and torsional modes show interesting trends that are not apparent from the characteristics of undeformed cantilever beams (see, for example, Minguet and Dugundji[1]). The influence of the large static deflections on the modes is found by linearizing the governing equations of motion around a given static position to yield the small amplitude vibrations of the beam around that large static position.

In the present analysis, the amplitudes of motion are also allowed to be large, and emphasis is given on how the vibrational behavior of the blades is affected by not only the static tip deflection but also the amplitude level at the tip. The structural information from this type of free vibration analysis, such as frequency vs amplitude and mean position vs amplitude, should give insight when predicting more general aeroelastic behavior where large periodic forcing functions or nonlinear aerodynamic loads due to dynamic stall could contribute to large amplitude limit cycle motion. Flexible helicopter blades (or high aspect ratio fixed wings) are good examples in which these nonlinearities could play important roles and lead into nonlinear large amplitude self-excited stall flutter. The present analysis is drawn from a more general aeroelastic investigation involving structural and aerodynamic stall nonlinearities reported by Kim[2] and should serve as an introduction to the understanding of such complex phenomena.

Two types of nonlinear helicopter blade equations can be available for the purpose of present analysis; equations based on various geometrical ordering schemes and ones not based on ordering schemes. The former group of equations approximate large displacements and rotations mostly up to second order[3,4] and the latter group preserve the complete nonlineari-

ties in them.[1,5] The nonlinear equations derived by Minguet and Dugundji,[1] which fall in the latter group, are used here. All assumptions made there are retained throughout this analysis. As indicated by Friedmann,[6] this model does not include shearing and warping deformation, but for the purposes of current analysis the model is adequate to show the basic characteristics of large amplitude free vibration of composite helicopter blades.

A new technique based on harmonic balance and iterative Newton-Raphson algorithm is introduced to solve for the modes and their frequencies as functions of amplitudes of interest under moderate to large static deflections. Results of numerical analysis are presented for a $[0/90]_{3S}$ lay-up of graphite/epoxy composite beam under various static deflections, and results for a $[45/0]_S$ lay-up are briefly discussed.

Also, to illustrate the efficiency of the present modeling, a simple modal analysis based on the nonlinear equations of motion for moderate deflections developed by Hodges and Dowell[3] and Boyd[4] has been performed for the $[0/90]_{3S}$ lay-up, a case where no structural couplings exist. The results are compared against those of the present modeling.

Finally, a series of experiments similar to the one performed by Minguet and Dugundji[1] using several cantilevered composite blades was performed, and is shown to confirm the validity of the modeling.

Basic Differential Equations

There are 12 first-order, nonlinear differential equations that describe the statics and dynamics of composite blades completely. For thorough derivation of the equations see Minguet and Dugundji.[1] All the equations are derived based on the following transformation matrix that transforms the global coordinate x, y, z into the local one ξ, η, ζ (see Fig. 1), i.e.,

$$\begin{Bmatrix} i_\xi \\ i_\eta \\ i_\zeta \end{Bmatrix} = [T] \begin{Bmatrix} i_x \\ i_y \\ i_z \end{Bmatrix}$$

$$[T] = \begin{bmatrix} \cos\beta\cos\psi & \cos\beta\sin\psi & \sin\beta \\ -\cos\theta\sin\psi - \sin\theta\sin\beta\cos\psi & \cos\theta\cos\psi - \sin\theta\sin\beta\sin\psi & \sin\theta\cos\beta \\ \sin\theta\sin\psi - \cos\theta\sin\beta\cos\psi & -\sin\theta\cos\psi - \cos\theta\sin\beta\sin\psi & \cos\theta\cos\beta \end{bmatrix} \tag{1}$$

Here, ψ, β, and θ are the local Euler angles. The transformation matrix is orthogonal and related to the rotation or curvature matrix as follows:

$$[T]^{-1} = [T]^T$$
$$\frac{\partial [T]}{\partial s} = [\kappa][T] \tag{2}$$

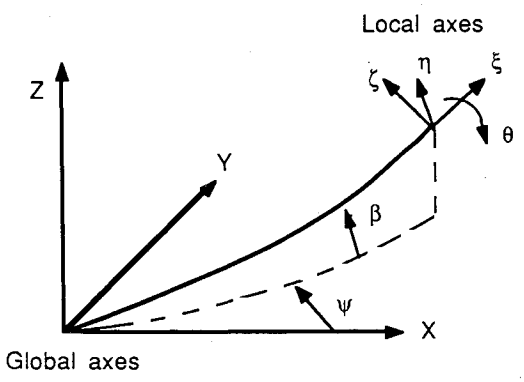

Fig. 1 Definition of global and local axes.

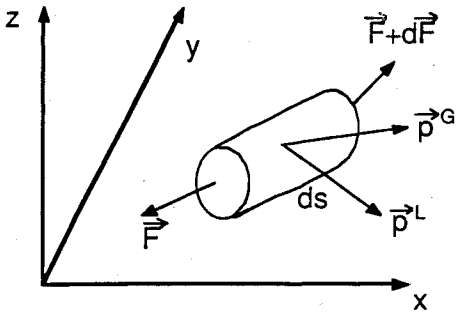

Fig. 2 Definition of local internal forces (moments defined similarly).

with

$$[\kappa] = \begin{bmatrix} 0 & \kappa_\zeta & -\kappa_\eta \\ -\kappa_\zeta & 0 & \kappa_\xi \\ \kappa_\eta & -\kappa_\xi & 0 \end{bmatrix} \tag{3}$$

where

$$\kappa_\xi = \frac{\partial\theta}{\partial s} + \sin\beta\frac{\partial\psi}{\partial s}$$
$$\kappa_\eta = -\cos\theta\frac{\partial\beta}{\partial s} + \sin\theta\cos\beta\frac{\partial\psi}{\partial s} \tag{4}$$
$$\kappa_\zeta = \sin\theta\frac{\partial\beta}{\partial s} + \cos\theta\cos\beta\frac{\partial\psi}{\partial s}$$

Inverting the above differential equation yields

$$\frac{\partial\theta}{\partial s} = \kappa_\xi - \sin\theta\tan\beta\kappa_\eta - \cos\theta\tan\beta\kappa_\zeta$$
$$\frac{\partial\beta}{\partial s} = -\cos\theta\kappa_\eta + \sin\theta\kappa_\zeta \tag{5}$$
$$\frac{\partial\psi}{\partial s} = \frac{\sin\theta}{\cos\beta}\kappa_\eta + \frac{\cos\theta}{\cos\beta}\kappa_\zeta$$

The global displacements x, y, and z are related to Euler angles via

$$\frac{\partial x}{\partial s} = (1+\epsilon)\cos\beta\cos\psi$$
$$\frac{\partial y}{\partial s} = (1+\epsilon)\cos\beta\sin\psi \tag{6}$$
$$\frac{\partial z}{\partial s} = (1+\epsilon)\sin\beta$$

where ϵ is the axial strain along the reference line.

In addition to the above six compatibility equations, one has to consider equilibrium of forces and moments of the beam (see Fig. 2). The first three differential equations that describe the equilibrium of the local force resultants are

$$\frac{\partial F_1}{\partial s} - \kappa_\zeta F_2 + \kappa_\eta F_3 + T_{11}p_x + T_{12}p_y + T_{13}p_z + p_1 = 0$$
$$\frac{\partial F_2}{\partial s} + \kappa_\zeta F_1 - \kappa_\xi F_3 + T_{21}p_x + T_{22}p_y + T_{23}p_z + p_2 = 0 \tag{7}$$
$$\frac{\partial F_3}{\partial s} - \kappa_\eta F_1 + \kappa_\xi F_2 + T_{31}p_x + T_{32}p_y + T_{33}p_z + p_3 = 0$$

The other three differential equations describe the equilibrium of the local moment resultants M_1, M_2, M_3.

$$\frac{\partial M_1}{\partial s} - \kappa_\xi M_2 + \kappa_\eta M_3 + T_{11}m_x + T_{12}m_y + T_{13}m_z + m_1 = 0$$

$$\frac{\partial M_2}{\partial s} + \kappa_\zeta M_1 - \kappa_\xi M_3 + T_{21}m_x + T_{22}m_y + T_{23}m_z + m_2 - F_3 = 0 \tag{8}$$

$$\frac{\partial M_3}{\partial s} - \kappa_\eta M_1 + \kappa_\xi M_2 + T_{31}m_x + T_{32}m_y + T_{33}m_z + m_3 + F_2 = 0$$

In helicopter problems, generally two kinds of loadings arise: inertial loads that include the linear and angular accelerations, Coriolis, centrifugal, and gravitational forces and the aerodynamic loads that include both steady and unsteady parts. The former group usually appears as the global p_G, m_G and the latter group appears as the local p_L, m_L. In the present analysis, only the linear and angular inertial and the gravitational loads are included in order to consider the nonrotating free vibration case. Hence for a blade without mass centroid offset

$$\begin{aligned} p_x &= -m\ddot{x} \\ p_y &= -m\ddot{y} \\ p_z &= -m\ddot{z} - mg \\ m_x &= m_y = m_z = 0 \end{aligned} \tag{9}$$

and

$$\begin{aligned} p_1 &= p_2 = p_3 = 0 \\ m_1 &= -I_p\ddot{\phi} \simeq -I_p\ddot{\theta} \\ m_2 &= m_3 \simeq 0 \end{aligned} \tag{10}$$

For formulation of rotating free vibration, one needs to add, in addition to the above terms, the centrifugal and Coriolis forces in the global p_x, p_y, p_z and m_x, m_y, m_z (see Kim[2] for the formulation of these loads).

Finally, a set of generalized stress-strain relations are incorporated via the following six linear equations.

$$\begin{bmatrix} F_1 \\ F_2 \\ F_3 \\ M_1 \\ M_2 \\ M_3 \end{bmatrix} = \begin{bmatrix} E_{11} & E_{12} & E_{13} & E_{14} & E_{15} & E_{16} \\ & E_{22} & E_{23} & E_{24} & E_{25} & E_{26} \\ & & E_{33} & E_{34} & E_{35} & E_{36} \\ & & & E_{44} & E_{45} & E_{46} \\ & \text{SYM} & & & E_{55} & E_{56} \\ & & & & & E_{66} \end{bmatrix} \begin{bmatrix} \epsilon \\ \gamma_{\xi\eta} \\ \gamma_{\xi\zeta} \\ \kappa_\xi \\ \kappa_\eta \\ \kappa_\zeta \end{bmatrix} \tag{11}$$

Here $\gamma_{\xi\eta}$ and $\gamma_{\xi\zeta}$ represent the two transverse shear strains. In its most general case, the above stiffness matrix can be full, i.e., there can be couplings between all of three force resultants, three moment resultants, and all of six strain components. However, in consistency with the earlier assumptions of a Bernoulli-Euler beam, the calculations of the two shear strains are completely ignored in the current analysis.

Equations of Motion for Moderate Deflections

Unlike the 12 first-order, complete nonlinear differential equations just presented, an alternative group of equations in the variables v, w, and θ is often used to represent the blade motion. In these, large displacements and angles are approximated usually up to second order, with the resulting equations valid only for moderate range of deflections, whether static or dynamic.

In the early work by Hodges and Dowell[3] and Boyd[4] these equations were derived by considering the total energy expression of equilibrium in global frame. Both derivations lead to the same results provided that a consistent ordering scheme is maintained throughout. A third derivation was obtained by the authors[7] through a direct reduction of the 12 nonlinear differential equations based on the same ordering scheme employed by Hodges and Dowell, Boyd, and others.

The moderate deflection equations of motion can appear in several different forms, but the ones used in the analysis are as follows[4]:

$$\begin{aligned} w\text{:}\quad & [(EI_\eta w'') + (EI_\zeta - EI_\eta)(v''\theta + w''\theta^2)]'' - (w'F_x)' \\ & = p_{zT} + m'_{yT} \\ v\text{:}\quad & [EI_\zeta v'' + (EI_\zeta - EI_\eta)(w''\theta - v''\theta^2)]'' - (v'F_x)' \\ & = p_{yT} - m'_{zT} \\ \phi\text{:}\quad & -(GJ\phi')' + (EI_\zeta - EI_\eta)[(w''^2 - v''^2)\theta + v''w''] = m_{1T} \end{aligned} \tag{12}$$

where one has

$$\begin{aligned} \theta &\simeq \phi - \int_0^x w'v''\,dx \\ F_x &\simeq -\int_x^L p_{xT}\,dx \\ \epsilon &\simeq u' + v'^2/2 + w'^2/2 = 0 \end{aligned} \tag{13}$$

In the above, no structural couplings and mass centroid offset have been introduced. This form shows more clearly the type of nonlinear couplings involved between the w, v, and ϕ motions. These nonlinear couplings depend on the difference in bending stiffness $(EI_\zeta - EI_\eta)$, and would give rise to linear couplings even for small amplitude vibrations by the presence of initial static deflections in w and v. Although the moderate deflection Eqs. (12) lend themselves well to Galerkin solutions, a sufficient number of modes must be used to capture the nonlinear effects when static deflections are present. As seen later, this also holds for large amplitude vibration cases. At any rate, they can always be checked against the general solution of the 12 nonlinear differential equations.

Modeling of Large Amplitude Motion

In large amplitude vibration problems, the natural frequency of a particular mode can be a function of amplitude of that mode. Furthermore, a certain amount of coupling may exist between the static and dynamic components of various variables. Thus two basic characteristics that distinguish the nonlinear, large amplitude vibration from the linear, small vibration can be summarized as 1) the natural frequency of a particular mode changes as its amplitude increases and 2) the mean position of the beam can also change as a function of amplitude.

For the purpose of present analysis, all quantities are assumed in the following form

$$X(\omega, t) = X_0(\omega) + X_S(\omega)\sin \omega t$$

where X_0 and X_S represent the static part and the associated amplitude around that static part, respectively. The fact that X_S is not a small quantity is reflected in the frequency dependency of both X_0 and X_S.

The analytic modeling consists of substituting the above expression for each variable into the 12 governing equations. As a result of multiplications involving $\sin \omega t$, this process will produce many higher order terms containing higher harmonics such as $\sin 2\omega t$, and $\sin 3\omega t$ (see the Appendices). A harmonic balance method is then employed to retain only terms that are constants and coefficients of $\sin \omega t$. All the higher harmonic terms are left out. An ordering scheme that keeps magnitudes of up to third order is employed to maintain a consistent level of nonlinearities in all of the equations (see the Appendices).

It is emphasized that this ordering scheme does not mean

$$\cos\theta \sim 1 - \theta^2/2 + \text{H.O.T.}$$

but rather

$$\cos\theta \sim \cos\theta_0 - \sin\theta_0\Delta\theta - \tfrac{1}{2}\cos\theta_0(\Delta\theta)^2 + \tfrac{1}{6}\sin\theta_0(\Delta\theta)^3 + \text{H.O.T.}$$

where $\theta = \theta_0 + \Delta\theta$, and the θ_0 and $\Delta\theta = \theta_s \sin\omega t$ represent the static and dynamic components of θ. So the complete nonlinearity in the large rotations is still kept in a static sense, but as a strategy, terms only up to third order are kept in the dynamic counterparts.

Occasionally, a second harmonic is included in the solution to check the validity of the first harmonic solution and search for any missing motion of higher harmonic content. It is found that including terms involving the second harmonic cos $2\omega t$, in two-dimensional bending is enough to capture the missing second harmonics in the fore-and-aft modes. In other words, only F_1, F_3, M_2, and β, x, z are expressed in the form

$$X(\omega, t) = X_0(\omega) + X_S(\omega)\sin\omega t + X_{2C}(\omega)\cos 2\omega t$$

with all other variables containing only the constants and the first harmonics as before. This is done based on the intuition that second harmonics will mostly appear in x_s and z_s, and their motion should be initially 90 deg out of phase with the rest of the amplitudes. These second harmonic amplitudes will then capture the so-called *rocking* of motion in the fore-and-aft modes. A new set of formulas that performs multiplications of harmonics is implemented accordingly. These are different from the ones in the Appendices in that they now have to deal with cos $2\omega t$ as well.

As for equations of motion for moderate deflections, the same procedure can be performed, leaving only constant and sin ωt terms in the variables v, w, θ. Then an appropriate modal solution can be sought by applying Galerkin's method. For details of the formulation, see Kim.[2]

Method of Solution

Having obtained the necessary formulations for the large amplitude, nonlinear free vibration model, one can express the earlier equations in vector form

$$\frac{\partial X_0}{\partial s} = g_0(X_0, X_S, \omega) \qquad (14)$$

$$(12\times 1) \qquad (12\times 1)$$

and

$$\frac{dX_S}{ds} = g_0(X_0, X_S, \omega) \qquad (15)$$

$$(12\times 1) \qquad (12\times 1)$$

where

$$X_0 = [F_{10}\ F_{20}\ F_{30}\ M_{10}\ M_{20}\ M_{30}\ x_0\ y_0\ z_0\ \theta_0\ \beta_0\ \psi_0]^T$$

$$X_S = [F_{1s}\ F_{2s}\ F_{3s}\ M_{1s}\ M_{2s}\ M_{3s}\ x_s\ y_s\ z_s\ \theta_s\ \beta_s\ \psi_s]^T$$

The two vector function arrays g_0 and g_s contain many product terms involving multiplications of two or three harmonic quantities. Multiplications of harmonics and calculations of the coefficients of the resulting new harmonics can be easily implemented according to the formulas in the Appendices.

To solve this system, the 24 equations (now 12 for the static part, 12 for the dynamic part) are integrated from the tip to the root of the blade using a Runge-Kutta algorithm. In the numerical integration, one has to guess boundary values of displacements and rotations at the tip as well as the frequency that will make, for a given mode shape, all the displacements and rotations at the root as close to the prescribed values as possible. A linear solution by Minguet and Dugundji[1] can provide a good guess for these values. The functional relationships between the two sets of boundary values at the root and at the tip can be written as

$$X_r = f(X_t, \omega) \qquad (16)$$

$$(12\times 1) \qquad (12\times 1)$$

where

$$X_t = [x_0\ x_s\ y_0\ y_s\ z_0\ z_s\ \theta_0\ \theta_s\ \beta_0\ \beta_s\ \psi_0\ \psi_s]^T$$

at the tip, and

$$X_r = [0\ 0\ 0\ 0\ 0\ 0\ \theta_0\ 0\ \beta_0\ 0\ \psi_0\ 0]^T$$

at the root. Here θ_0, β_0, and ψ_0 are the prescribed values at the root (they are zero for flat cantilever blades). Since the initial guess for the 12 components of X_t is not perfect, there will be nonzero residues R when the integration reaches the root. A Newton-Raphson type algorithm can then be used to produce a better set of tip boundary values based on the current values. This will produce the following set of boundary values,

$$X_t^{n+1} = X_t^n - J(X_t^n, \omega^n)^{-1}R^n \qquad (17)$$

where

$$R^n \equiv f(X_t^n, \omega^n) - X_r$$

$$j: \quad (12\times 12) \text{ Jacobian matrix}$$

and the subscript n refers to the nth iterative values. The nth boundary values X_t^n at the tip will eventually march to the true solution, provided it exists. If the second harmonic terms cos $2\omega t$ are included as described earlier, the resulting Jacobian is then (15×15). Note that a (18×18) Jacobian would result if all of the variables contain the second harmonic terms.

It is noted that whatever algorithm is used, it must take iterations on the frequency as well as the boundary values, since the frequency of a mode will vary with amplitude level. Therefore, one of the six boundary amplitudes at the tip x_s, y_s, z_s θ_s, β_s, or ψ_s, is replaced by the frequency ω, and the replaced displacement is fixed throughout iterations. If bending modes are of concern, z_s will be fixed; if they are torsional modes, then θ_s is fixed, and so on. The iteration will march until the boundary conditions at the root are met, i.e., the residues R^n are zeros or at least less than some preset ϵ where $\epsilon \ll 1$.

It should be remembered that the above solution procedure, when applied to linear problems, is similar to the so called transfer matrix technique used to obtain helicopter blade vibration modes by Isakson and Eisley.[8]

In case of using moderate deflection equations, there will result in general, $6N$ nonlinear algebraic equations provided that the same number N of modes are used for both static and dynamic parts of v, w, and θ in the Galerkin's approximation. A similar Newton-Raphson technique then can be employed. Note that the integration in space is not needed here. One can reduce the number of equations by observing that for the bending modes, v and θ equations are not required, while for the fore-and-aft or torsional modes in the dynamic part, the sin ωt term does not exist in w (true only for the cases without structural couplings).

Analytic Results

The prescribed algorithms have been used to investigate the first and second bending ($1B$, $2B$) modes, first fore-and-aft ($1F$) modes, and first torsion ($1T$) modes of cantilevered

blades with the lay-ups $[0/90]_{3S}$, $[45/0]_S$ of graphite/epoxy for various static tip deflections. The configurations of the blades investigated are those used by Minguet and Dugundji[1] (560 mm long, 30 mm wide).

The static deflections were varied by imposing and adjusting uniform gravity level throughout the blade. As stated earlier, the z_s, y_s, and θ_s were fixed for bending, fore-and-aft, and torsional modes, respectively. Also, θ_0, β_0, and ψ_0, at the root were all set equal to zero since the blade is a flat cantilevered beam. A total of 16 equally distributed node points were used along the blade. The linear mode shapes and their natural frequencies provided reasonable trial values which, after a few iterations, led to nontrivial solutions. Each analysis was continued until the amplitude could not be further increased. At this point, the Jacobian matrix became almost singular and the solution did not converge.

The first example is the $[0/90]_{3S}$ specimen. The natural frequencies of linear modes for this case as obtained by Minguet and Dugundji[1] are given in Fig. 3. Figures 4–7 show mode shapes at two extreme amplitude levels under initial static tip deflection 59 mm. For comparison, nondimensional mode values with major component equal to unity at the tip have been plotted against nondimensional span values for each pair of mode shapes. It is seen that for most of the amplitude range, the nonlinear modes remain almost unchanged from the linear modes in their shapes. Next, Figs. 8 and 9 show change of natural frequencies as functions of tip amplitudes z_s, y_s, and $\theta_s L$ at two different initial static tip deflections, 59 mm and 210 mm. Figures 10 and 11 represent the variations of the tip centershifts z_0 (mean vertical position at the tip) of various modes as functions of the tip amplitudes. Also presented in Figs. 8–11 as dashed curves are the results from a nonlinear analysis of the moderate deflection equations, using Galerkin's method along with harmonic balance. Here, to stress the moderateness of the nonlinearities in the

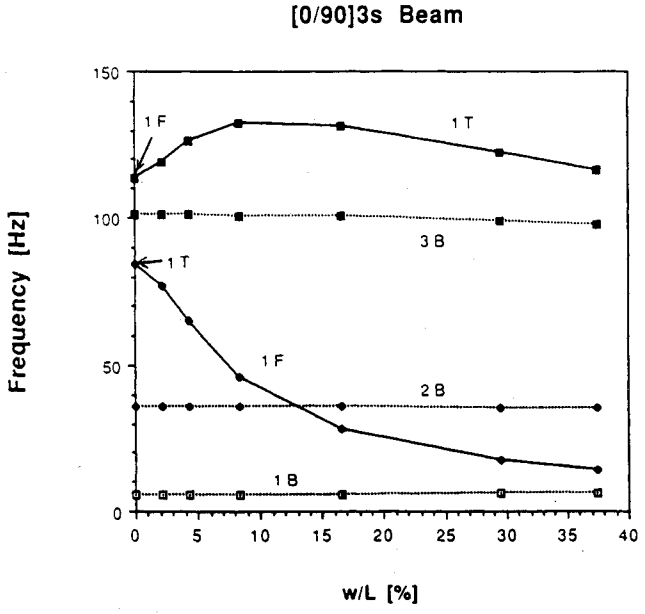

Fig. 3 Natural frequencies of $[0/90]_{3S}$ beam as a function of static tip deflection (from Ref. 1).

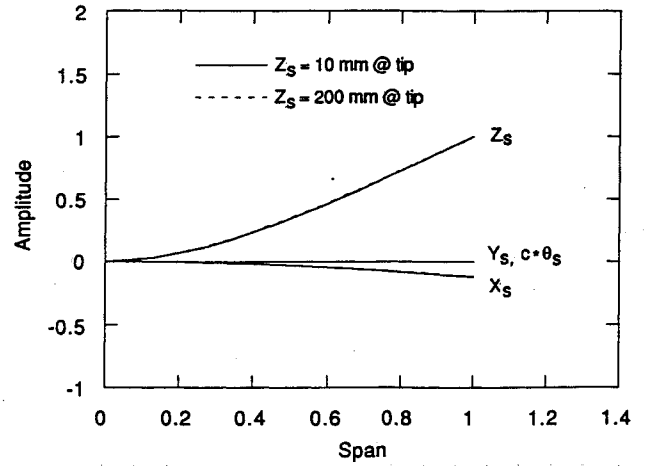

Fig. 4 First bending modes; $[0/90]_{3S}$, 59 mm static tip deflection.

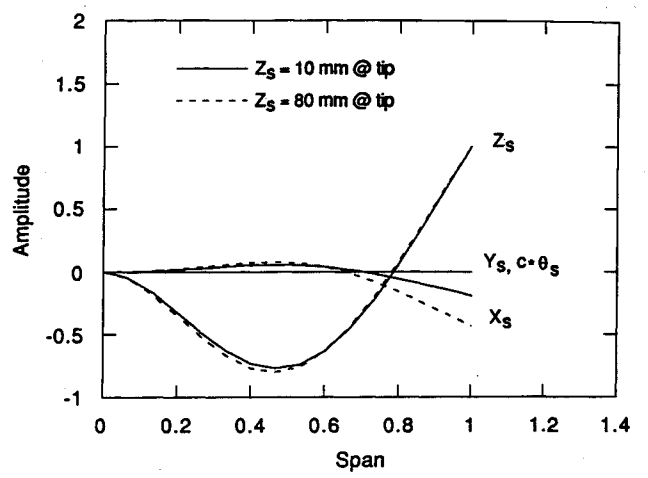

Fig. 5 Second bending modes; $[0/90]_{3S}$, 59 mm static tip deflection.

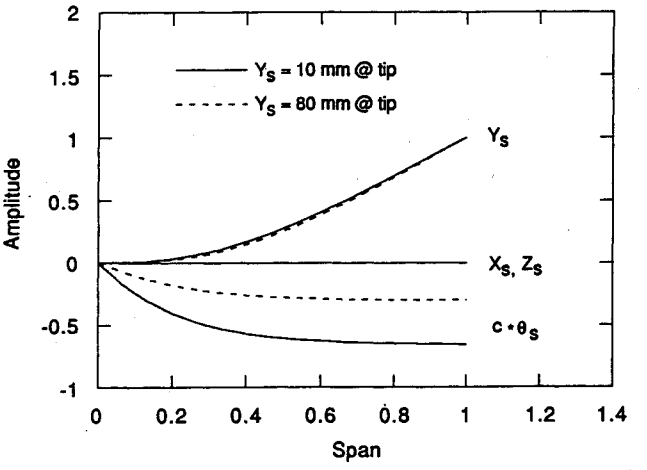

Fig. 6 First fore-and-aft modes; $[0/90]_{3S}$, 59 mm static tip deflection.

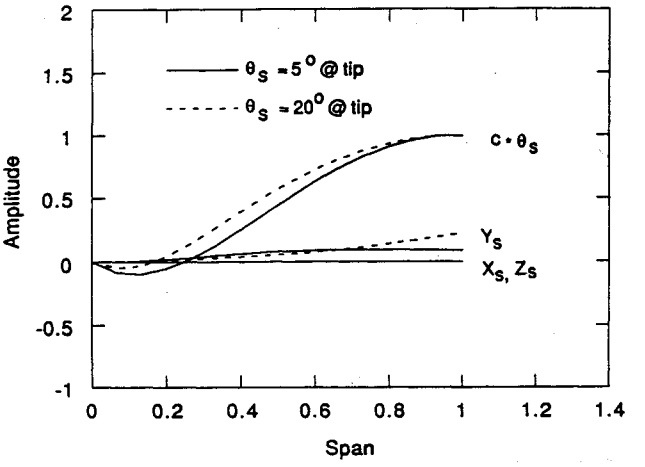

Fig. 7 First torsion modes; $[0/90]_{3S}$, 59 mm static tip deflection.

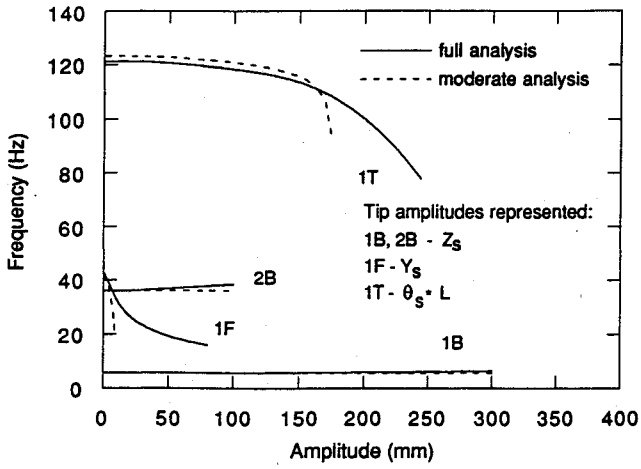

Fig. 8 Frequncy vs amplitude; $[0/90]_{3S}$, 59 mm static tip deflection.

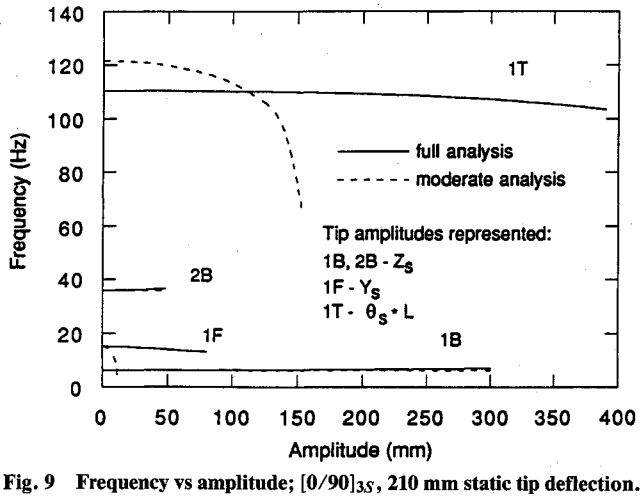

Fig. 9 Frequency vs amplitude; $[0/90]_{3S}$, 210 mm static tip deflection.

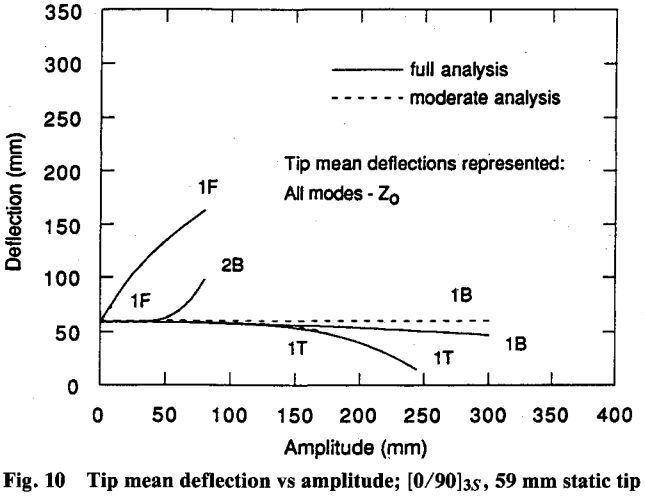

Fig. 10 Tip mean deflection vs amplitude; $[0/90]_{3S}$, 59 mm static tip deflection.

governing equations, the dashed curves are referred to as "moderate analysis" and the solid curves as "full analysis." The bending and torsional modes employed in the Galerkin's method in the moderate analysis were those for straight beams without initial static deflection.[9] It was found that at least three modes for each of v_s, θ_s were necessary to ensure accuracy in predicting linear $1F$ and $1T$ modes when initial static tip deflections were present. A total of four modes was used for each of w_0, v_s, θ_s in the present analysis. From Figs. 8–11, the following two observations can be made.

1) Increasing amplitude level has slight stiffening effects in $1B$and $2B$ modes, whereas it has significant softening effects in $1F$ and $1T$ modes, particularly for a moderate range of initial static tip deflections. As a result, the natural frequencies of bending modes rise slightly with amplitude level and those of $1F$ and $1T$ modes always drop.

2) The previous frequency changes are accompanied by centershift changes. Increasing the amplitude levels has a slight effect on the centershifts of bending modes except for the $2B$ mode, whereas it has a significant centershift increase for the $1F$ mode and a centershift decrease for the $1T$ mode, particularly for moderate static tip deflections.

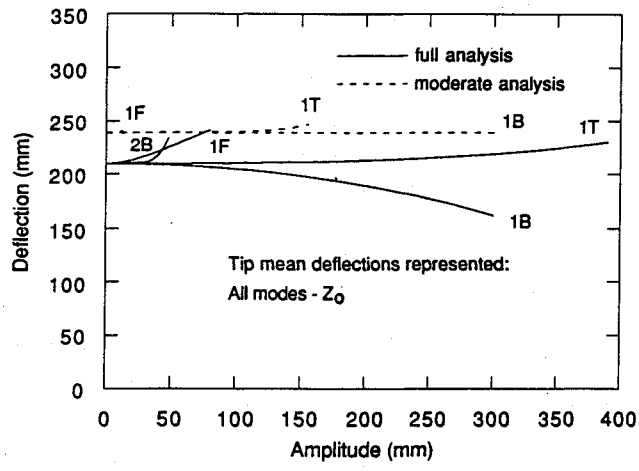

Fig. 11 Tip mean deflection vs amplitude; $[0/90]_{3S}$, 210 mm static tip deflection.

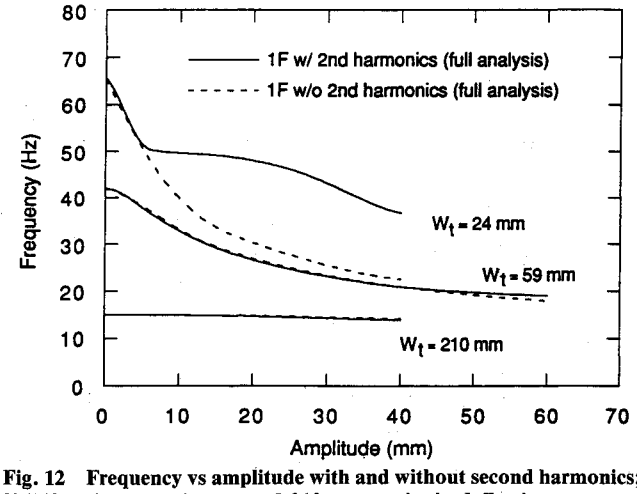

Fig. 12 Frequency vs amplitude with and without second harmonics; $[0/90]_{3S}$, 24 mm, 59 mm, and 210 mm static tip deflection.

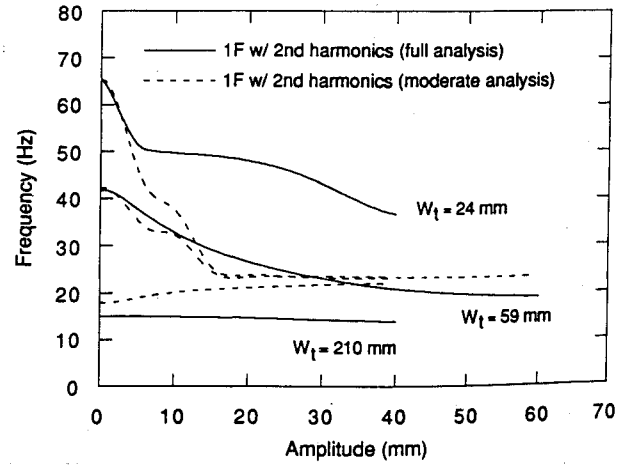

Fig. 13 Frequency vs amplitude with second harmonics; $[0/90]_{3S}$, 24 mm, 59 mm, and 210 mm static tip deflection.

Figure 12 represents the effects of second harmonics on the $1F$ modes at three different static tip deflections, 24 mm, 59 mm, and 210 mm. These were obtained using the fully nonlinear equations. Also presented for comparison are results without the second harmonics. From the plot, $1F$ modes exhibit significant second harmonic rocking motion effects at moderate to large amplitude levels when the static tip deflection is small. On the other hand, when the static tip deflection is moderate to large, the effects of the second harmonics are almost negligible. An effort was made to seek for any second harmonics in $1T$, $1B$, and $2B$ modes, but they have been found very weak and are not presented here.

Figure 13 shows the effects of including second harmonics in the moderate analysis for the $1F$ mode. It is seen that the moderate analysis gets improved and can yield larger amplitude motion, but the results still deviate significantly from the full analysis.

From these observations, it is believed that to improve the moderate analysis for large amplitude vibration, an ordering scheme higher than second order and/or inclusion of higher harmonics might be needed.

The second example investigated is that of $[45/0]_S$, which exhibits bending-torsion coupling. Only the qualitative aspects of the numerical results are discussed here. Due to the structural coupling, computer time was increased and the convergence became more sensitive. This resulted in earlier breakdown of the Jacobian matrix, which in turn caused a shorter range of solutions available as functions of amplitudes. Once again, the mode shapes did not change significantly from the linear modes. Despite the existing bending-torsion coupling, the two former observations 1) and 2) can again be made. The effects of second harmonics on the $1F$ modes was also weak except at the small static tip deflection level.

Experiment

Several flat beams of various lay-ups were tested dynamically to verify the analytical model presented. The beam specimens, which are 560 mm by 30 mm, were all borrowed from a test site where Minguet and Dugundji[1] set up their previous experiment. The major goal of the vibration tests was to observe the effects of large amplitudes on the frequencies and mean tip deflections of various vibrational modes in the presence of initial static tip deflections.

The test equipment recruited was basically the same as before, but to ensure large amplitude motion, a tiny T-shaped lever was attached on the bottom of the blades near the root. The shaker was then connected to the lever horizontally via a soft spring, and hence was able to excite large amplitude motion in fore-and-aft and torsional modes. To excite a large amplitude bending motion, this type of setup was not necessary and the shaker was directly connected to the bottom of the blades vertically, via a soft spring. For more details of the experimental setup, see Kim.[2] The amplitudes of the blades were gradually increased by amplifying the signal from the function generator. At each amplitude level, the shaking frequency was adjusted so as to yield the maximum motion, whereby a nonlinear resonance state was achieved. This peak resonance at a specific frequency was believed to simulate a large amplitude free vibration in a best possible manner. The frequency then was read and the corresponding amplitude as well as the mean vertical position at the tip were measured visually.

Experimental Results

All of the specimens exhibited certain degrees of initial curvatures due to residual strains created during the manufacturing processes. Hence, these inherent curvatures combined

Table 1 Experimental frequency and tip mean deflection; $[0/90]_{3S}$

	$[0/90]_{3S}$, 39 mm static tip deflection[a]					
1B mode:						
Ampl., mm	linear	16	44	80	120	
Freq., Hz	5.6 (5.8)	5.5 (5.8)	5.5 (5.8)	5.5 (5.8)	5.5 (5.9)	
Z_0, mm	39 (39)	38 (39)	36 (39)	36 (39)	34 (38)	
2B mode:						
Ampl., mm	linear	6	12	19	25	—
Freq., Hz	35 (36)	35 (36)	35 (36)	34 (36)	34 (36)	—
Z_0, mm	39 (39)	38 (39)	37 (39)	36 (40)	36 (40)	—
1F mode:						
Ampl., mm	linear	—	1.7	24	39	—
Freq., Hz	54 (55)	—	34 (30)	30 (26)	25 (22)	—
Z_0, mm	39 (39)	—	78 (79	92 (92)	122 (123)	—

[a]Experiment—solid; analysis—( ).

Table 2 Experimental frequency and tip mean deflection; $[0/90/0]_S$

	$[0/90/0]_S$, 57 mm static tip deflection[a]					
1B mode:						
Ampl., mm	linear	21	50	73	110	
Freq., Hz	3.0 (3.6)	3.0 (3.6)	3.0 (3.6)	2.9 (3.6)	2.9 (3.6)	
Z_0, mm	57 (57)	60 (57)	58 (57)	59 (56)	54 (56)	
2B mode:						
Ampl., mm	linear	6	13	19	23	—
Freq., Hz	19 (22)	19 (22)	19 (22)	18 (22)	18 (22)	—
Z_0, mm	57 (57)	59 (57)	59 (57)	59 (57)	58 (58)	—
1F mode:						
Ampl., mm	linear	8	—	22	32	65
Freq., Hz	25 (26)	22 (21)	—	17 (15)	15 (13)	12(—)
Z_0, mm	57 (57)	66 (71)	—	94 (97)	115 (116)	179 (—)
1T mode:						
Ampl., deg	linear	6.5	10	15	20	—
Freq., Hz	83 (75)	83 (74)	— (73)	— (70)	— (65)	—
Z_0, mm	57 (57)	57 (57)	— (57)	— (56)	— (49)	—

[a]Experiment—solid; analysis—( ).

Table 3 Experimental frequency and tip mean deflection; $[0/90]_S$

$[0/90]_S$, 176 mm static tip deflection[a]						
1B mode:						
Ampl., mm	linear	35	73	100		
Freq., Hz	2.2 (2.7)	2.2 (2.7)	2.2 (2.8)	2.1 (2.8)		
Z_0, mm	176 (176)	178 (175)	168 (174)	163 (172)		
2B mode:						
Ampl., mm	linear	7	10	—		
Freq., Hz	13.0 (16.0)	12.9 (16.0)	12.8 (16.0)	—		
Z_0, mm	176 (176)	176 (176)	176 (176)	—		
1F mode:						
Ampl., mm	linear	14	48	55	68	
Freq., Hz	7.6 (6.9)	7.3 (6.7)	7.4 (6.0)	7.4 (5.8)	7.2 (5.6)	
Z_0, mm	176 (176)	183 (178)	210 (193)	216 (197)	226 (203)	
1T mode:						
Ampl., deg	linear	14	25	29	33	—
Freq., Hz	43 (44)	43 (44)	44 (44)	44 (44)	44 (44)	—
Z_0, mm	176 (176)	178 (177)	185 (179)	189 (180)	197 (181)	—

[a]Experiment—solid; analysis—( ).

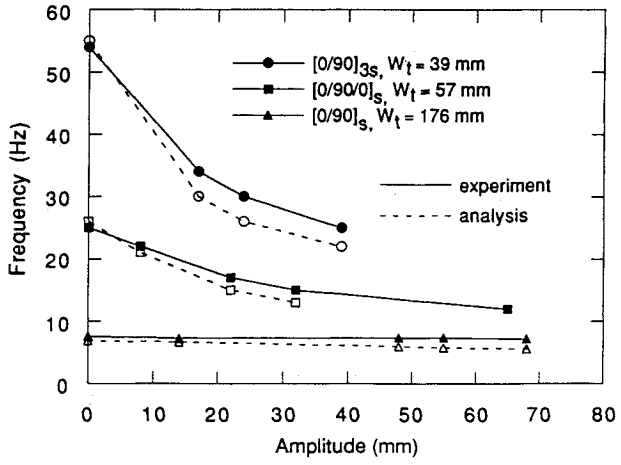

Fig. 14 Experimental frequency vs amplitude; first fore-and-aft modes.

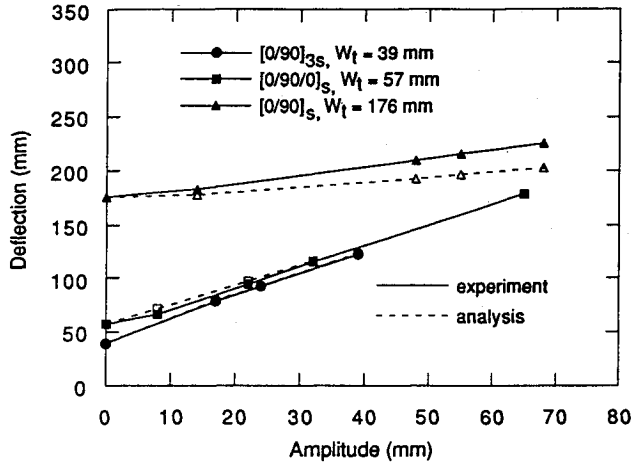

Fig. 15 Experimental tip mean deflection vs amplitude; first fore-and-aft modes.

with gravity could be used to create initial static deflections in the blades. It was felt that influences of initial static deflections and large amplitudes would be much more critical than structural couplings as evident from the analytic results. Hence, most tests concentrated on specimens that do not have structural couplings. Test specimens chosen were $[0/90]_{3S}$, $[0/90/0]_S$, $[0/90]_S$, and $[45/0/45]_S$. The initial tip deflections of these lay-ups ranged from 39 mm to 176 mm. Tables 1–3 show the results of the dynamic tests for $[0/90]_{3S}$, $[0/90/0]_S$, and $[0/90]_S$ with 39 mm, 57 mm, and 176 mm of static tip deflection, respectively. Analytic results from the full analysis with second harmonics included are also shown in parentheses for comparison.

Except for first bending modes, there were some ranges of amplitudes that did not allow pure vibrational modes due to interaction of, or parametric or combinatory resonances between, several modes. Such instances are indicated as hyphens in the tables. Incidentally, the interference was most severe in $2B$ and $1T$ modes and in some cases, it was impossible to increase the tip amplitudes enough so as to observe any changes in the centershifts in these modes. On the contrary, $1B$ and $1F$ modes did not have such problems in most ranges of interest. Analytic results were not obtainable in some cases due to the singularity of the solution. These are also indicated as hyphens.

Figures 14 and 15 represent a variation of the experimental frequency and tip mean deflection of $1F$ modes with amplitude compared against analytic results. Note the large drop and rise in the experimental frequencies and tip mean deflections, respectively, as confirmed by analysis.

As seen in the tables and the figures, there is generally a good agreement between analysis and experiment within the ranges of amplitudes tested. From an aeroelastic point of view, it is $1F$, the fore-and-aft (lead-lag) mode that is most critical in determining stability and any nonlinear limit cycles of the blade, and the current test results are able to capture basic key aspects of large amplitudes vibration in that context.

Conclusions

The nonlinear analysis derived from the work by Minguet and Dugundji, and based on the use of Euler angles together with a harmonic balance, finite difference solution, seems an efficient technique for determining the nonlinear large amplitude free vibration of composite rotor blades.

It has been shown that both large static deflection and large amplitude can affect significantly the fore-and-aft modes and torsion modes, but not much the bending modes. More specific conclusions are as follows:

1) Increasing the amplitude level has slight stiffening effects in bending modes whereas it has significant softening effects in the $1F$, $1T$ modes, particularly for moderate range of initial static tip deflections. As a result, the natural frequencies of bending modes rise slightly while those of $1F$ and $1T$ modes always drop. The $1F$ in particular shows a large drop with amplitude level at moderate static tip deflections.

2) Increasing the amplitude level of a particular mode also results in centershift changes that are small for the bending modes but significant for the $1F$ and $1T$ modes, particularly for moderate initial static tip deflections. The $1F$ centershift seems to increase considerably with amplitude level.

3) The flat $[90/0]_{3S}$ or any isotropic blade with zero root angle has significant second harmonic contents in the $1F$ mode at small static tip deflections. These appear mostly in the bending amplitude z_s.

4) It appears that modal analysis based on a traditional second ordering scheme may not model the large amplitude vibration adequately.

5) Experiments on large amplitude blade vibration confirm the general trends of the analyses, particularly for the fore-and-aft modes.

Appendix A: Calculation of Coefficients of Harmonic Quantities

Recall that many of the terms in the equations involve trigonometric functions and their arguments are the three Euler angles ψ, β, and θ. It is clear that one can not apply the harmonic balance method with the Euler angles expressed as $x(\omega, t) = x_0(\omega) + x_s(\omega)\sin \omega t$ and themselves inside the trigonometric functions. So, it is useful to rely on series expansion versions of these trigonometric functions. To get the series expressions, let x represent any of the three Euler angles, and let $X(x)$ be any trigonometric function, i.e., $\cos x$, $\sin x$, $\tan x$, or $1/\cos x$. Then substituting

$$x = x_0 + x_s \sin \omega t$$

into the function X and expanding in a Taylor series about x_0 yields

$$X(x) = X(x_0) + \frac{dX}{ds}(x_0)x_s \sin \omega t + \frac{1}{2!}\frac{d^2X}{dx^2}(x_0)x_s^2 \sin^2\omega t$$

$$+ \frac{1}{3!}\frac{d^3X}{dx^3}(x_0)x_s^3 \sin^3\omega t + \text{H.O.T.} = X_0 + X_S \sin \omega t$$

$$+ X_{S2} \sin^2\omega t + X_{S3} \sin^3\omega t + \text{H.O.T.} \tag{A1}$$

where

$$X_0 \equiv X(x_0) \tag{A2}$$

$$X_S \equiv \frac{dX}{dx}(x_0)x_s \tag{A3}$$

$$X_{S2} \equiv \frac{1}{2!}\frac{d^2X}{dx^2}(x_0)x_s^2 \tag{A4}$$

$$X_{S3} \equiv \frac{1}{3!}\frac{d^3X}{dx^3}(x_0)x_s^3 \tag{A5}$$

Here according to our ordering scheme only terms up to third order are kept in the expansion. Then, when applying harmonic balance methods, the $\sin^2\omega t$ and $\sin^3\omega t$ can be expanded into constant and $\sin\omega t$ type terms after multiplication with other harmonic quantities, as shown in Appendix B.

Appendix B: Multiplication of Two Harmonic Quantities

In Appendix A it was seen that any harmonic quantity can be expressed, up to third order, as

$$X = X_0 + X_S \sin \omega t + X_{S2} \sin^2\omega t + X_{S3} \sin^3\omega t \tag{B1}$$

where X_0, X_S, X_{S2}, X_{S3} are determined by the formulas in Eqs. (A2–A5). $X(x)$ could be either a harmonic variable itself (e.g., $F, M, x, \ldots$) or a trigonometric function. If it is a harmonic variable S_{S2} and X_{S3} are identically zero. Now let's consider a product of two quantities, X and Y, which are expressed as above. It can be shown that

$$XY = (X_0 + X_S \sin \omega t + X_{S2} \sin^2\omega t + X_{S3} \sin^3 \omega t)$$

$$\cdot (Y_0 + Y_S \sin \omega t + Y_{S2} \sin^2\omega t + Y_{S3} \sin^3 \omega t)$$

$$= (XY)_0 + (XY)_S \sin \omega t + (XY)_{S2} \sin^2 \omega t$$

$$+ (XY)_{S3} \sin^3\omega t \tag{B2}$$

where

$$(XY)_0 \equiv X_0Y_0$$

$$(XY)_S \equiv X_0Y_S + X_SY_0$$

$$(XY)_{S2} \equiv X_0Y_{S2} + X_SY_S + X_{S2}Y_0$$

$$(XY)_{S3} \equiv X_0Y_{S3} + X_SY_{S2} + X_{S2}Y_S + X_{S3}Y_0$$

When applying harmonic balance method only the static and the first harmonic terms are retained. For this purpose note that

$$\sin^2\omega t = \tfrac{1}{2} - \tfrac{1}{2} \cos 2\omega t \tag{B3}$$

$$\sin^3 \omega t = \tfrac{3}{4} \sin \omega t - \tfrac{1}{4} \sin 3\omega t \tag{B4}$$

So after neglecting higher harmonics one gets

$$XY = [(XY)_0 + \tfrac{1}{2}(XY)_{S2}] + [(XY)_S + \tfrac{3}{4}(XY)_{S3}]\sin \omega t \tag{B5}$$

Some of the governing equations contain products of three harmonic quantities. Multiplication of three harmonics X Y and Z can be performed as a series of two multiplications involving two harmonic quantities as $XYZ = (XY)Z$, where the harmonics of (XY) are obtained according to Eq. (B2).

Acknowledgment

This research was performed in the Technology Laboratory for Advanced Composite (TELAC) of the Department of Aeronautics and Astronautics at the Massachusetts Institute of Technology, supported under U.S. Army Research Office Contract DAAL03-87-K-0024 with Gary Anderson as technical monitor.

References

[1]Minguet, P. J., and Dugundji, J., "Experiments and Analysis for Composite Blades Under Large Deflections. Part 1: Static Behavior, Part 2: Dynamic Behavior," *AIAA Journal,* Vol. 28 Sept. 1990, pp. 1573–1588.

[2]Kim, T., "Nonlinear Large Amplitude Structural and Aeroelastic Behavior of Composite Rotor Blades at Large Static Deflection," Ph.D. Thesis, Dept. of Aeronautics and Astronautics, Massachusetts Inst. of Technology, Cambridge, MA, May 1992.

[3]Hodges, D. H., and Dowell, E. H., "Nonlinear Equations of Motion for the Elastic Bending and Torsion of Twisted Non-Uniform Rotor Blades," NASA TN D-7818, Dec. 1974.

[4]Boyd, W. N., "Effect of Chordwise Forces and Deformations and Deformations due to Steady Lift on Wing Flutter," Dept. of Aeronautics and Astronautics, Stanford Univ., SUDAAR 508, Stanford CA, Dec. 1977.

[5]Hodges, H., Hopkins, A. S., Kunz, D. L., and Hinant, H. E., "Introduction to GRASP—General Rotorcraft Aeromechanical Stability Program. A Modern Approach to Rotorcraft Modeling," *Journal of the American Helicopter Society,* Vol. 32, April 1987, pp. 78–90.

[6]Friedmann, P. P., "Helicopter Rotor Dynamics and Aeroelasticity: Some Key Ideas and Insights," *Vertica,* Vol. 14, No. 1, 1990, pp. 101–121.

[7]Kim, T., and Dugundji, J., "Nonlinear Large Amplitude Vibration of Composite Helicopter Rotor Blade at Large Static Deflections," Dept. of Aeronautics and Astronautics, Massachusetts Inst. of Technology, TELAC Rept. 90-14, July 1990.

[8]Isakson, G., and Eisley, J. G., "Natural Frequencies in Coupled Bending and Torsion of Twisted Rotating and Nonrotating Blades," NASA CR-65, July 1964.

[9]Meirovitch, L., *ELements of Vibration Analysis,* McGraw-Hill, New York, 1975.